Nanotribology of carbon nanotubes

2008 J. Phys.: Condens. Matter 20 365214

(http://iopscience.iop.org/0953-8984/20/36/365214)

J. Phys.: Condens. Matter **20** (2008) 365214 (14pp) doi:10.1088/0953-8984/20/36/365214

Nanotribology of carbon nanotubes

Bharat Bhushan

Nanoprobe Laboratory for Bio- and Nanotechnology and Biomimetics,
Ohio State University, 201 W. 19th Avenue, Columbus, OH 43210-1142, USA

E-mail: bhushan.2@osu.edu

Received 30 June 2008, in final form 23 July 2008
Published 19 August 2008
Online at stacks.iop.org/JPhysCM/20/365214

Abstract

Carbon nanotubes (CNTs) have remarkable mechanical and electrical properties which make them attractive for a large number of applications. Attempts have been made to develop reinforced composites, super-strong fibers and sheets, nanoprobes, chemical and biological sensors, nanoscale electromechanical devices and molecular electronics. Nanotube arrays are being developed for field-emitter-based screens and thermal management. The mechanical strength of many of these devices critically relies on the nanotribology and nanomechanics of CNTs. Various investigations of adhesion, friction, wear and mechanics of MWNTs, SWNTs and MWNT arrays have been carried out. This paper provides an overview.

(Some figures in this article are in colour only in the electronic version)

1. Introduction

Carbon nanotubes (CNTs), since their discovery in 1991 by Iijima (1991), have attracted intensive research activities due to their remarkable mechanical and electrical properties (Dresselhaus *et al* 2000). They exist in two forms: single-walled nanotubes (SWNTs) made of one atomic plane of carbon atoms perfectly rolled into a cylinder, and multi-walled nanotubes (MWNTs), made of concentric cylindrical cells of graphene (sheets of graphite-like arrangement of C atoms) where the intershell interaction is predominantly van der Waals. CNTs inherit the high stiffness and high strength of the basal plane of graphite while preserving its low density (Robertson *et al* 1992, Treacy *et al* 1996, Wong *et al* 1997, Salvetat *et al* 1999, Yu *et al* 2000). With their tubular structure and graphite-like sp^2 bonds, CNTs can sustain repetitive large deformation without catastrophic failure (Yakobson *et al* 1996, Falvo *et al* 1997). Their electronic properties can vary from metallic to semiconducting by changing their diameter and chirality (Wildoer *et al* 1998). They also have excellent thermal properties, making them suitable for thermal management of high power devices (Pambaguian *et al* 2007). Attempts have been made to develop reinforced polymeric composites (Thostenson *et al* 2001), super-strong fibers and sheets (Vigolo *et al* 2000, Jiang *et al* 2002, Dalton *et al* 2003, Zhang *et al* 2005), ultra-sharp resilient nanoprobes (Dai *et al* 1996), chemical and biological sensors (Wong *et al* 1998), nanoscale electromechanical devices (Baughman *et al* 1999, Kim and Lieber 1999) and molecular electronics (Tans *et al* 1998, Rueckes *et al* 2000, Collins *et al* 2001, Baughman *et al* 2002) based on CNTs. The vertical orientation of CNTs with respect to the substrate is used to increase the field emission of such nanostructures suitable for field-emission-based sensors for flat TV sets and computers (Fan *et al* 1999, Chen *et al* 2000, Nakayama and Akita 2001). CNT arrays also exhibit high thermal dissipation suitable for thermal management (Shaikh *et al* 2007). It is therefore of interest to study the aligned nanotube arrays.

We show an example of a CNT-based film and two sensors in which adhesion, friction and wear are important. Zhang *et al* (2005) produced highly oriented free-standing nanotube sheets as shown in figure 1(a). Individual MWNTs were drawn from a dense thicket of nanotube forest to create a long, horizontal array. The resulting ribbons were then layered atop one another to make a super-strong sheet. Mechanical properties of nanotube ribbons, such as elastic modulus and tensile strength, critically rely on the adhesion and friction between MWNTs. Figure 1(b) shows an SWNT biosensor. The conductance of CNT devices changes when proteins adsorb on the surface. The change in electrical resistance is a measure of protein adsorption. For high performance, adhesion should be strong between adsorbents and SWNTs. Figure 1(c) shows a schematic of a nanotube biosensor. It consists of a cantilevered CNT resting on another CNT supported at its two ends. Cellular forces applied at the free end of the nanotube cantilever are detected as the imbalance of current flowing through the nanotube bearing supporting the nanotube cantilever. The deflection of the nanotube cantilever involves

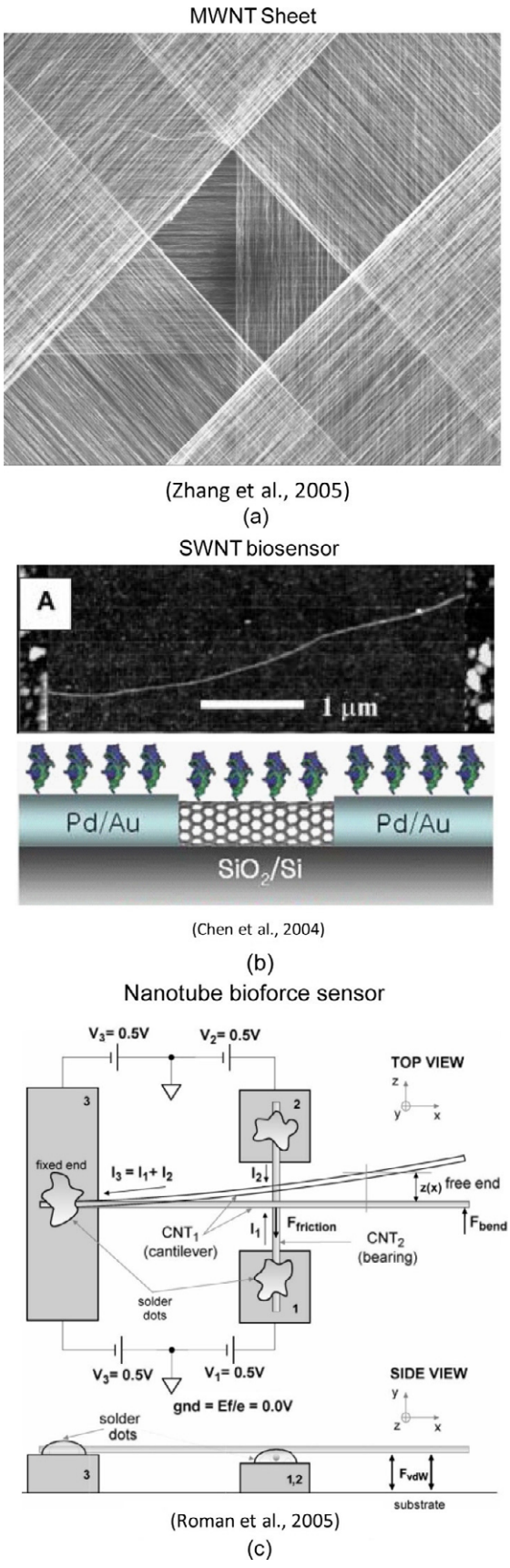

Figure 1. (a) SEM micrograph of an MWNT sheet (Zhang *et al* 2005), (b) SEM micrograph of an SWNT biosensor: the bottom schematic shows the adsorption of protein molecules on the SWNT (Chen *et al* 2004), and (c) schematic of a CNT bioforce sensor (Roman *et al* 2005).

inter-tube friction, which will modify the amplitude of thermal fluctuations in the region of the junction. These and many other applications demonstrate the importance of nanotribology and nanomechanics of CNTs.

The mechanical properties of the CNTs have been studied using theoretical and experimental methods. Mechanical robustness and nonlinear elastic responses of nanotubes and nanorods have been analyzed by various researchers (Robertson *et al* 1992, Iijima *et al* 1995, Treacy *et al* 1996, Yakobson *et al* 1996, Falvo *et al* 1997, Wong *et al* 1997, Salvetat *et al* 1999, Ru 2000, Belytschko *et al* 2002, Nakajima *et al* 2003). Yu *et al* (2000) analyzed the breaking mechanism of MWNTs under tensile loads, while Daraio *et al* (2004a, 2004b) focused on the dynamic nanofragmentation mechanism, the nonlinear contact interaction and the impact response of carbon nanotube forests. Cao *et al* (2005) reported the fully reversible compressive behavior of CNT films. Besides the analysis of the mechanical properties, the understanding of the nanotribological behavior, such as the adhesion and the friction between the CNTs and CNTs against different materials, plays a key role in the exploration of new applications for the CNTs (Bhushan 2002, 2008). The direct nanotribological characterization of nanotubes is scarce. Bhushan *et al* (2008a) carried out adhesion, friction and wear as well as bending measurements for a multi-walled nanotube (tip) sliding on Si, Al and mica surfaces. Using an atomic force microscope (AFM), they also performed experiments on a commercial Si tip sliding on SWNT and MWNT arrays. Bhushan *et al* (2008b) and Bhushan and Ling (2008) studied adhesion and friction of an MWNT tip sliding on an SWNT bridge suspended on a micro-trench. In this paper, we present a summary of adhesion, bending, friction and wear studies of CNTs.

2. Experimental details

2.1. AFM tips

MWNT AFM tips used for the experiments were prepared by mounting an individual MWNT on the tip of a conventional Si AFM probe using a micro-manipulator operated under an inverted microscope (Nguyen *et al* 2005). Low-density and individually separated MWNTs were grown by chemical vapor deposition (CVD) on a Pt wire coated with a liquid catalyst solution. A single MWNT with a typical length greater than 10 μm was transferred to the tip of an Si cantilever coated with a 15 nm Ni film. When the nanotube and the Si tip were in close proximity, an electrical potential of 1–2 V was applied to improve the alignment of the nanotube with respect to the apex of the Si tip, and then by increasing the voltage to 10 V and above, the MWNT was detached from its source at the point of defects. The applied voltage caused local heating at the MWNT–Ni-coated-Si-tip interface, which strengthens the interface via physical welding of the MWNT and the Ni-coated Si tip. The diameter of the MWNT tips typically ranged from 10–30 nm. The MWNTs were open, since their diameter was relatively large for cap closing to occur. The total height of the tip, including the supporting silicon tip structure and the length

of the attached MWNT tip, was approximately 17 μm, with the length of the nanotube protruding beyond the Si apex to be about 2 μm, as seen in figure 2(a). The tips are reported to be hydrophobic. The cantilever had a resonance frequency of about 75 kHz and nominal spring constant of 2 N m^{-1}.

Force-modulation-etched single-crystal silicon tips (RFESP, Veeco) and silicon nitride tips (NP-S, Veeco) were also used for measurements (Bhushan 2008). The square pyramidal silicon tip was held by a cantilever with a nominal resonance frequency of 75 kHz and nominal spring constant of 3 N m^{-1}; nominal tip radius was about 10 nm. The square pyramidal silicon nitride tip was held by a cantilever with 0.58 N m^{-1} nominal spring constant; nominal tip radius was 20 and 50 nm.

2.2. CNT arrays

Two different vertically aligned carbon nanotube arrays were tested, as shown in figure 2(b). One array is composed of SWNTs, with diameters less than 5 nm. The second array is formed by MWNTs, with diameters between 20 and 50 nm. For the two arrays, the length of the nanotubes is between 5 and 10 μm. The nanotubes are open with no capping. The aligned SWNTs were synthesized by deposition of ∼1 nm Fe on Al (∼10 nm)-coated SiO_2/Si substrate, followed by plasma-enhanced vapor phase deposition (PECVD). After the synthesis, the SWNTs were transferred onto a sputtered gold film, followed by ∼10% HF aqueous solution etching (Huang *et al* 1999). To prepare an aligned MWNT/polymer sample, polystyrene (PS) film was first placed on the top surface of a vertically aligned carbon nanotube array on an SiO_2/Si substrate (Huang *et al* 1999). By heating the SiO_2/Si substrate by an underlying hot plate to a temperature above T_m and below T_c, the melted PS film gradually filtrated into the nanotube forest through a combined effect of the gravity and capillary forces. The infiltration depth (i.e. the embedment length) of PS into the nanotube forest depends strongly on the temperature and heating time. After a predetermined heating time, the polymer-infiltrated nanotube array was peeled off from the SiO_2/Si substrate in an aqueous solution of HF (10% wt) to generate a free-standing film of vertically aligned carbon nanotubes embedded into the PS matrix (Qu and Dai 2007).

2.3. SWNT bridge suspended on micro-trench

SWNT bridges were synthesized by catalytic thermal chemical vapor deposition in a low pressure furnace (Jungen *et al* 2006, 2007). Prior to the CVD growth, microchips were fabricated by surface micromachining of 1.5 μm thick polycrystalline silicon (poly-Si) layers. The poly-Si layers were uniformly coated with a bimetallic thin film of 8 nm Al and 1 nm Ni by sputtering. The film thickness was monitored *in situ* by a quartz crystal microbalance. The chips were transferred in air and subjected to hydrogen pre-treatment at 0.02 MPa and 850 °C for 10 min to allow the reduction of nickel oxides and the formation of Ni islands. The latter serves as catalytic seeds for the growth of SWNTs under methane and hydrogen (3:1) at 0.02 MPa and 850 °C during 15 min. Heating and cooling were performed under vacuum, and the chamber was opened only after cooling to at least 250 °C. A typical SEM image of SWNTs suspended on top of a trench 2 μm wide and 1.5 μm deep is shown in figure 2(c) (Bhushan *et al* 2008b). The SWNTs appear taut and straight and some exhibit a branched structure. The average diameter of the suspended SWNT bridge was about 1.43 nm.

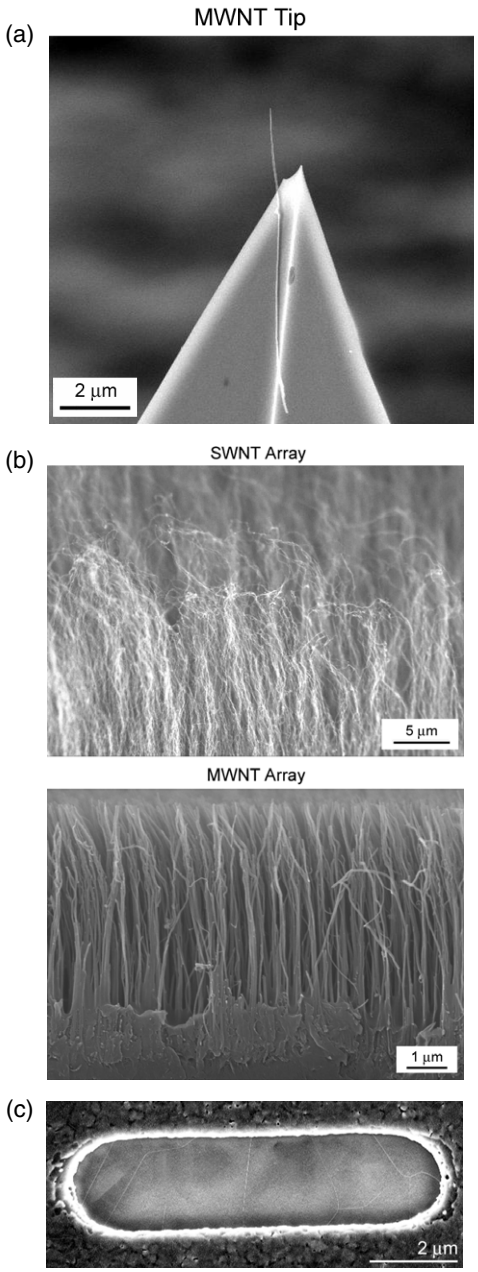

Figure 2. (a) SEM image of the MWNT tip (Bhushan *et al* 2008a), (b) SEM images of the vertically aligned SWNT and MWNT arrays. In the top image bundles of SWNTs are observed (Bhushan *et al* 2008a) and (c) SEM image of SWNT bridges suspended on the top of a micro-trench made of polycrystalline silicon (Bhushan *et al* 2008b).

To measure the adhesion and friction between nanotubes, the MWNT tip was brought into contact with the SWNT bridge and then scanned either in the lateral or vertical direction. The schematic of the experimental set-up is shown in figure 3. The

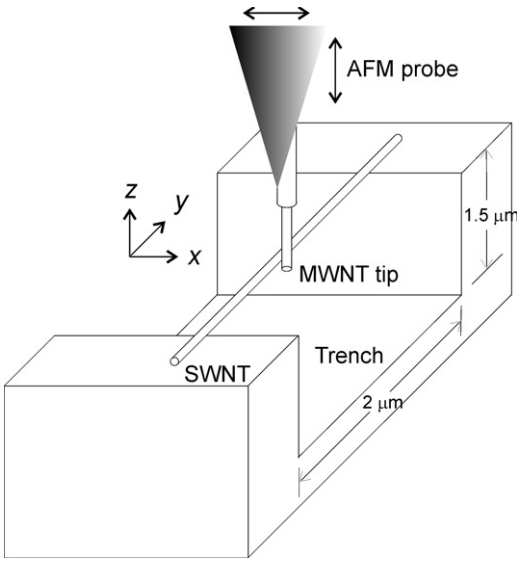

Figure 3. Schematic of the experimental set-up for nanotribological measurements between individual nanotubes. The double arrow indicates the ramping direction (x or z direction) (based on Bhushan *et al* 2008b and Bhushan and Ling 2008).

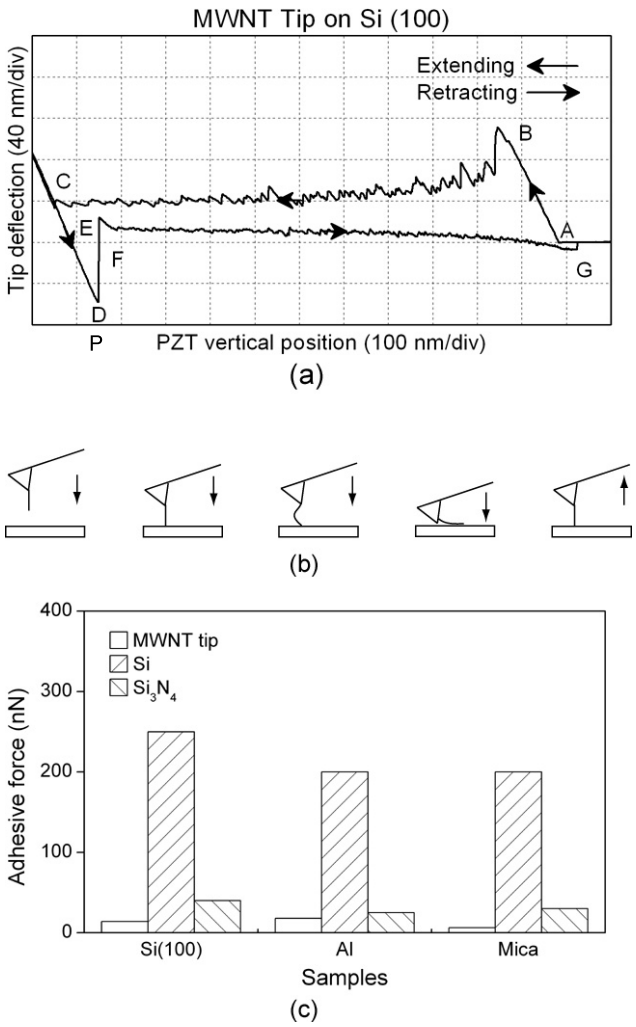

Figure 4. (a) Force versus distance curves using the MWNT tip on the Si sample, (b) schematics of the buckling of the MWNT tip during the application of compressive normal load in the force calibration mode and (c) mean values of the adhesive forces for various tips on Si, Al, and mica samples. The σ values are about 20% of the mean values.

longitudinal axis of the trench edge was aligned with the long axis of the AFM cantilever. During tapping mode imaging with an oscillating frequency of 47.5 kHz by manipulating the center and size of the scan area, the MWNT tip was positioned inside the trench and close to its ends. To bring the MWNT tip into contact with the SWNT bundle, the x offset was changed in a step of 50 nm while the oscillation amplitude of the AFM cantilever was monitored. An immediate drop of the oscillation amplitude indicated the contact between the MNWT tip and SWNT bundle. After contact, the tip was scanned in either the lateral or vertical direction for adhesion and friction measurements.

3. Adhesion, bending friction and wear of MWNT tips and SWNT and MWNT arrays

3.1. MWNT tips on flat surfaces

Adhesion, bending and friction between MWNT tips and single-crystal Si(100) and single-crystal aluminum and mica samples were carried out by Bhushan *et al* (2008a). Adhesion measurements were made using force calibration mode to capture force versus distance curves. The force versus distance curves of the MWNT tip on the Si(100) is shown in figure 4(a). It shows a nonlinear behavior that can be related to the effect of the tip–surface interactions. The nanotube on the tip comes in contact with the surface (point A). As the tip continues to be pressed, the contact force causes the linear deflection of the cantilever. After this initial bending, as the tip travels toward the sample (from B to C), the cantilever deflection (load) remains about constant with some variation. The nonlinear behavior indicates that, as the tip is continuously pushed into the surface, it induces the MWNT to bend and buckle, and the nanotube deflection is more than the cantilever deflection (figure 4(b)). It is noted that, during buckling, the graphitic C–C bonds, more specifically the π and σ bonds along the sp^2 hybridized chains, transform from the sp^2 to the sp^3 hybrid form when a mechanical stress is imposed along the nanotube axis. Such transformation is due to the breakage of the π bonds, and it is reversible since the sp^2 bonds are more thermodynamically stable than the sp^3 bonds (Tombler *et al* 2000). The nanotube buckles until the applied force reaches the Euler buckling force (Young and Budynas 2002):

$$F_{\text{Euler}} = (\pi^2 EI)/L^2 \tag{1}$$

where E is the MWNT Young's modulus (~1 TPa Wong *et al* 1997), I is the area moment of inertia ($I = \pi(r_2^4 - r_1^4)4$), where r_1 and r_2 are inner and outer radii of the nanotube ($r_2 \sim 10$ nm for the tip) and L is the nanotube length ~2 μm. Above the buckling force, the MWNT becomes unstable and buckles sideways, and lies on the surface and slides. The bucking force for the nanotube tip under study is calculated to be about 20 nN. This suggests that, since the load being applied

Table 1. Adhesive force and coefficient of friction for various tips on Si, Al and mica samples (based on Bhushan *et al* 2008a).

	F_{adh} (nN)			Coefficient of friction		
	Tips			Tips		
Sample	MWNT	Si	Si_3N_4	MWNT	Si	Si_3N_4
Si	14	250	40	0.05	0.05	0.05
Al	18	200	25	0.04	0.05	0.04
Mica	6.3	200	30	0.06	0.05	0.04

at point B (∼100 nN) is of the order of the buckling force, the nanotube buckles from point B to C and lies sideways. Friction between the nanotube and the surface with some roughness and continuous bending of the nanotube is responsible for the variations observed from point B to C.

At point C, the silicon tip supporting the MWNT snaps into contact with the surface, inducing a linear deflection of the cantilever. When the tip is retracted by the piezo (point D), the elastic force of the cantilever overcomes the adhesion between the silicon tip and the sample and the tip jumps out of contact (point E). Once the silicon tip jumps out of contact (point E), the elastic energy stored by the MWNT is released (from E to F). After that, the bent MWNT will gradually unload its stress accumulated earlier in the extending regime, when the tip continuously moves away from the sample. The MWNT tip detaches from the surface at point G. The adhesion force was obtained by multiplying the vertical distance between point G and the zero line to the cantilever stiffness, and the corresponding values are presented in figure 4(c) and table 1.

For comparison, the adhesive forces have also been measured using Si and Si_3N_4 tips, and the data are presented in figure 4(c) and table 1. The adhesion experienced by the silicon tip is the highest. This can be explained with the higher capillary force to which silicon is subjected to due to its low contact angle of 51° (Tao and Bhushan 2006a). Silicon nitride is characterized by a contact angle of 48° (Tao and Bhushan 2006b): therefore the adhesive force should have a magnitude compared to the one observed for the silicon tip. The difference in the adhesion may be related to the differences in surface energy based on the well-known surface energy theory of adhesion (Bhushan 2002, 2003).

For the MWNT tip sliding on different samples, the coefficient of friction has been evaluated and the data are presented in figure 5 and table 1. The coefficients of friction evaluated with the MWNT tip on the silicon and the mica surfaces are slightly higher than the values measured using the Si and the Si_3N_4 tips. Such a trend can be due to the surface chemistry and the bending of the nanotube during the scan. As the tip is pushed against the surface, the nanotube buckles and bends laterally, leading to an increase of the contact area, which causes higher resistance to tip motion.

The wear experiments were performed on a soft Au film using an MWNT tip at normal loads of 100 nN and 200 nN for 10 min. The wear experiments were also performed using Si tips for comparison. The gold film was 100 nm thick and was deposited on a silicon substrate by evaporation. The wear maps on the gold film are shown in figure 6 (Bhushan *et al* 2008a). It

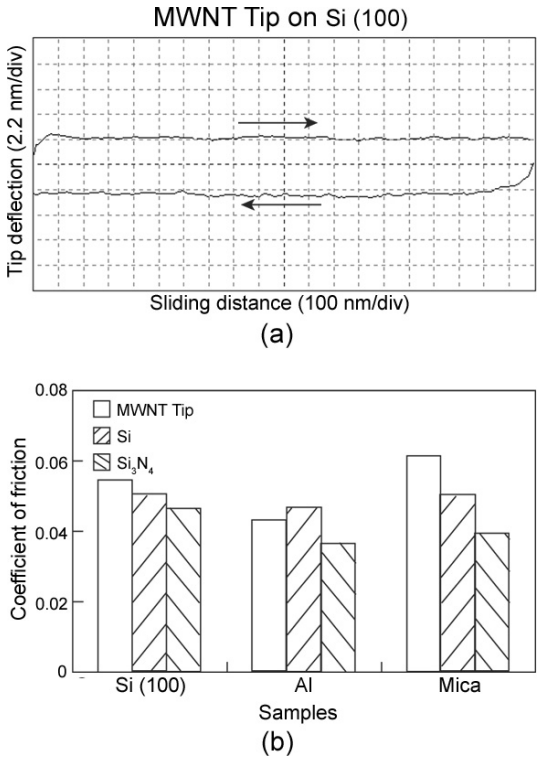

Figure 5. (a) Vertical deflection of the MWNT tip on the Si sample, sliding along the longitudinal axis of the cantilever beam for the friction measurement at a constant load of 100 nN, and (b) mean values of coefficients of friction for various tips on Si, Al and mica samples. The σ values are about 15% of the mean values (Bhushan *et al* 2008a).

is noted that the wear induced on the surface after the 100 nN normal load tests is very low and the material was pushed in the sliding direction of the tip. The topographical changes are more evident on the sample worn with the Si tip. In particular, it is hard to quantify a wear depth on the sample scanned with the MWNT tip, while the wear depth induced by the silicon tip is quantifiable and is about 3 nm. Low wear using the MWNT tip can possibly be due to the buckling of the carbon nanotube during the scan, which may be absorbing some of the force at contact, acting as a compliant spring moderating the impact of the tip on the surface (Larsen *et al* 2002, Nguyen *et al* 2005). Moreover, the smaller tip radius of the MWNT tip compared to the Si tip results in less contact area with the surface, which consequently does less damage (Bhushan 2002). By applying a 200 nN load, the damage induced to the gold film is about the same for the two tips used and the average wear depths are about 5 nm for both the MWNT and the Si tips. This result may suggest that, under such normal load, the silicon tip holding the MWNT may also be in contact with the surface, resulting in the similar wear behavior.

3.2. Si tips on SWNT and MWNT arrays

AFM images of SWNT and MWNT arrays are shown in figure 7 (Bhushan *et al* 2008a). The adhesion experiments were performed on the arrays using force calibration mode to capture force versus distance curves. The force versus

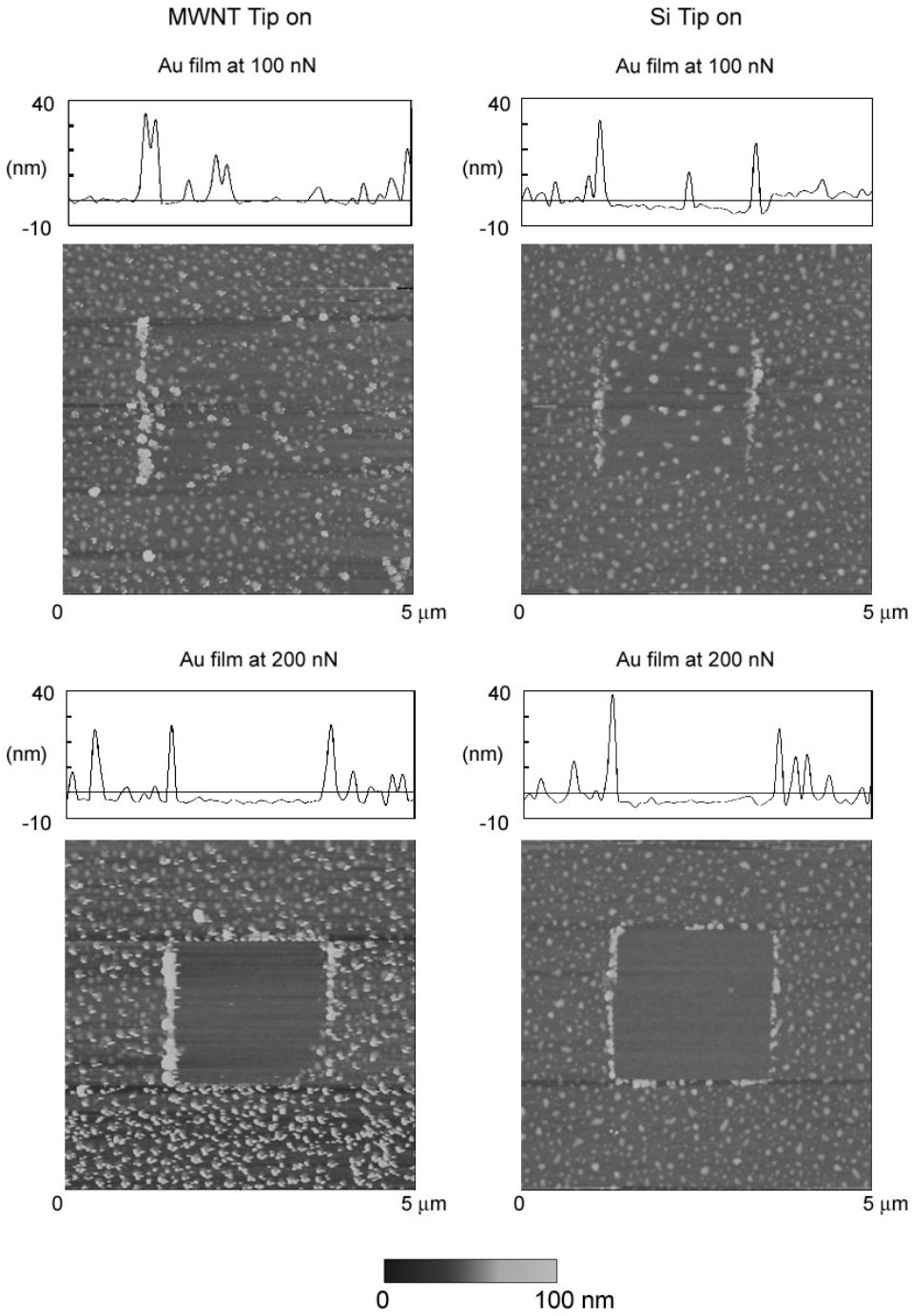

Figure 6. Tapping mode topographical images of the gold film after the wear test with the MWNT tip (in the left column) and the Si tip (in the right column) at normal loads of 100 and 200 nN for 10 min (Bhushan *et al* 2008a).

distance curves of the Si tip on the SWNT and MWNT arrays are shown in figure 8(a) (Bhushan *et al* 2008a). From these force plots it can be observed that, once the engagement occurs with the surface and the tip is pushed further, the cantilever is smoothly deflected until the piezo retraces in a nonlinear pattern, different from the linear pattern we usually observe on homogeneous samples. This can be explained as follows: as the tip is pushed further down in the array, more nanotubes get into contact with the tip, gradually contributing to repulsion. This condition is reversed when the tip is retracted from the arrays, leading to a nonlinear detaching curve. The source of the adhesive force is van der Waals forces in the contact of the tip with many carbon nanotubes or with a large contact area between the tip and a single nanotube due to its flexibility. Although the nanotubes are hydrophobic, the capillary force may still play a role in the adhesion between the silicon tip and the nanotube arrays due to the high surface energy of the nanotubes (Lau *et al* 2003). It has been shown that nanotube forests, with a 10–15 μm length, have an initial water contact angle of 161°; however, the droplets are not stable

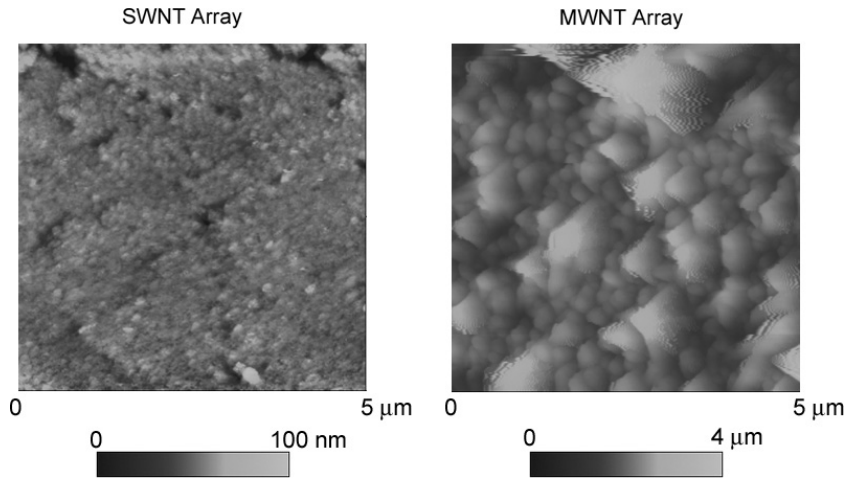

Figure 7. Tapping mode topographical images of the SWNT and MWNT arrays using an Si tip (Bhushan *et al* 2008a).

Table 2. Adhesive force and coefficient of friction for two Si tips on SWNT and MWNT arrays (Bhushan *et al* 2008a).

	F_{adh} (nN)		Coefficient of friction	
Sample	Si_1	Si_2	Si_1	Si_2
SWNT	86	96	0.29	0.20
MWNT	94	96	0.32	0.24

and eventually seep into the forest voids after a few minutes. For shorter CNTs, water droplets immediately seep into the voids and the nanotubes are even forced into bundles under the surface tension effects of the evaporating water between the nanotubes, reducing their hydrophobicity. The force versus distance curves monitored in this study are similar to the ones presented by Decossas *et al* (2001) on an MWNT carpet (where the nanotubes are not aligned) with a silicon nitride tip, and the data reported by Yurdumakan *et al* (2005) on an MWNT array with a silicon tip.

Some variability in the value of the adhesive force has been observed, and it is expected to be due to the different nanotube arrangements in different points of the samples including the packing density (figure 7). The data using the two tips are presented in figure 8(b) and table 2. The values for the SWNT array and MWNT array are comparable.

The friction data measured on the SWNT and MWNT arrays, using two Si tips, are shown in figure 9 and the values are reported in table 2 (Bhushan *et al* 2008a). The SWNT array exhibited a lower value of the coefficient of friction than that of the MWNT array, similar to the trends observed for the adhesion forces. Besides the density difference, the higher stiffness of the MWNTs, compared to the SWNTs, may contribute to the high friction. SWNTs have a smaller bending force constant, since their diameter is smaller. Thus they are mechanically more flexible than MWNTs and offer less resistance to the motion of the tip. Some influence may also occur by the cohesion forces between the nanotubes on the array, which is expected to be higher on the MWNT array since the nanotube density is higher than the density of the SWNT vertical array.

The wear experiments on the arrays were performed using Si tips at normal loads of 100 and 200 nN for 10 min. The surface topographical images of the SWNT and MWNT arrays captured after the wear tests are the same as in figure 7 (Bhushan *et al* 2008a), indicating that no apparent damage was caused on either sample. The tip profiles before and after the wear tests are presented in figure 10(a) (Bhushan *et al* 2008a). From this figure, it is possible to see how the Si tip wears. Whereas the changes in the shape of the tip are negligible on the SWNT array after the 100 and 200 nN tests, the shape of the tip changes with the MWNT array. It appears that the Si tip profile after tests with the MWNT array at 100 nN load gets sharper, which may be due to material pick-up. The flattening of the profiles at a distance of about 300 nm may occur due to artifacts in the silicon grating sample. Next, the wear volume of the tip generated by the MWNTs is calculated according to the procedure developed by Tao and Bhushan (2006a) and is found to be 34×10^4 nm^3 after the 100 nN normal load tests and 51×10^4 nm^3 after the 200 nN normal load experiments.

The friction force profiles obtained during the wear tests are presented in figure 10(b). The mean value of the friction force during the entire experiment is higher when the tip is scanned on the MWNT array. It is therefore reasonable to expect wear on the tip after the tests. The differences in the interactions with the SWNTs and MWNTs, and the fluctuations, have been discussed earlier.

4. Adhesion and friction between MWNTs and SWNTs

To measure adhesion and friction between nanotubes, the MWNT tip was brought into contact with the SWNT bridge and then ramped either in the lateral or vertical direction in a crossed geometry (Bhushan *et al* 2008b, Bhushan and Ling 2008). Lateral scanning works well for a flexible MWNT tip without catastrophic damage, whereas vertical scanning is also suitable for a stiff MWNT tip.

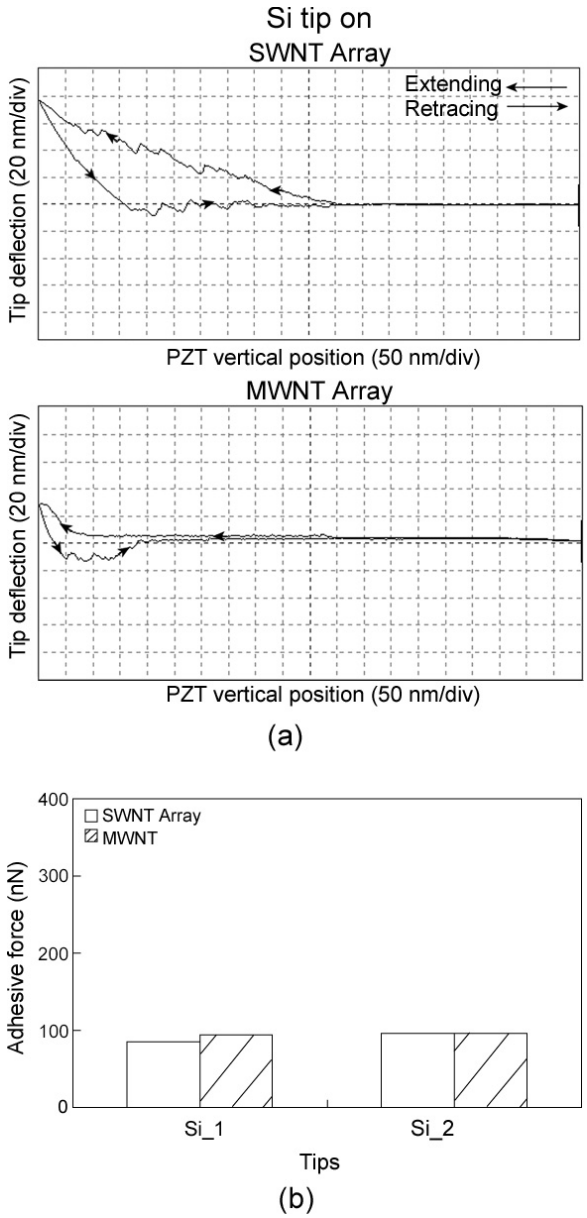

Figure 8. (a) Force versus distance curves of the Si tip on the SWNT and MWNT arrays, and (b) mean values of the adhesive forces measured with two different Si tips. The σ values are about 40% of the mean values (Bhushan *et al* 2008a).

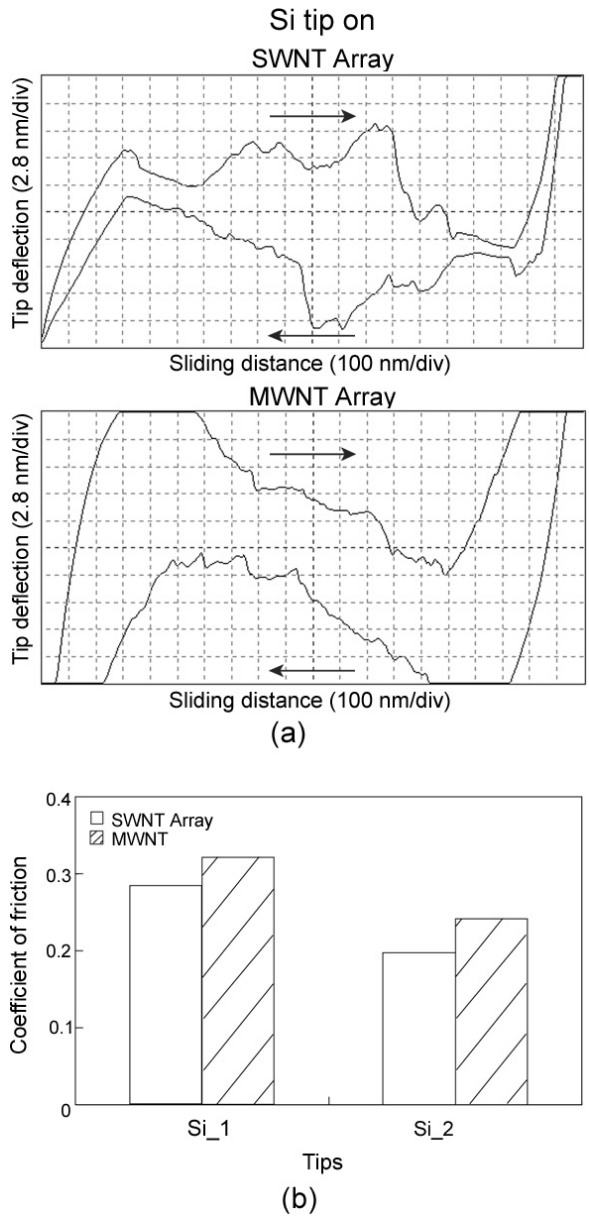

Figure 9. (a) Lateral deflection of the Si tip on the SWNT and MWNT arrays sliding along the axis orthogonal to the long axis of the cantilever beam for friction measurements and (b) mean values of the coefficients of friction measured with two different Si tips. The σ values are about 20% of the mean values (Bhushan *et al* 2008a).

4.1. Lateral scanning

In the lateral scanning experiments, the MWNT tip was scanned over the SWNT bridge, using an AFM operating in the tapping mode (Bhushan *et al* 2008b). The interaction between the two nanotubes changed the tapping amplitude and vertical deflection of the AFM cantilever. Compared to the vertical deflection signal, the change in the tapping amplitude signal is more sensitive to the very small dissipative friction force between nanotubes, and the latter is used to calculate the friction force. The tapping amplitude data during the initial contact of nanotubes are used for calculations; these data are used to avoid the influence on the friction from the normal force between nanotubes, which is expected to be small. Near the end of the scanning, the MWNT tip detached from the SWNT and the adhesive force between them caused significant changes to the vertical deflection of the cantilever, which is used to calculate the adhesive force between nanotubes. By dividing the friction force by the adhesive force, an experimental value of the coefficient of friction between nanotubes is determined. Using a continuum model, the contact size and the shear stress between nanotubes have been derived.

The MWNTs got stripped during scanning and became flexible and were thus suitable for lateral scanning experiments. Figure 11 shows cantilever tapping amplitude (a) and vertical deflection (b) for the MWNT tip over the trench

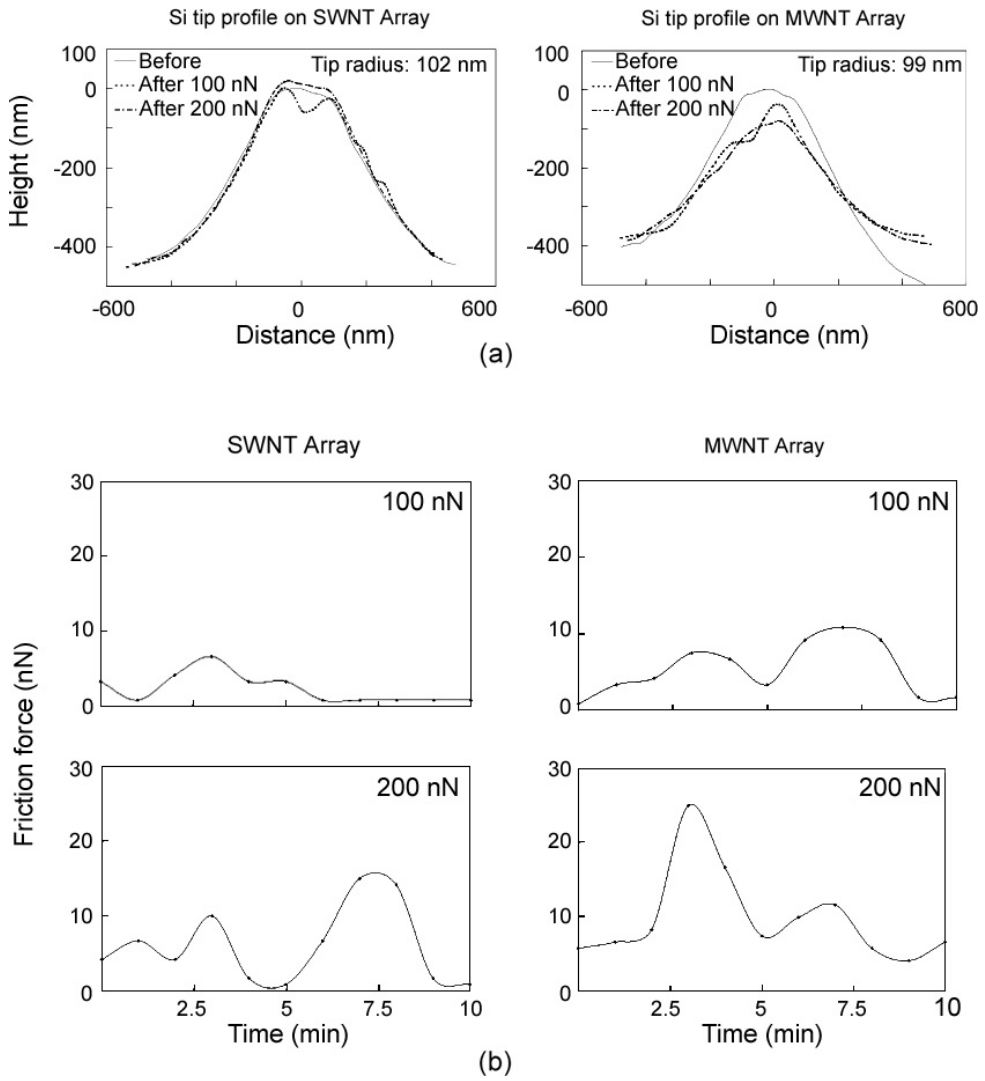

Figure 10. (a) Surface profiles of the Si tip before and after the wear tests on the SWNT and MWNT arrays at loads of 100 and 200 nN for 10 min and (b) friction force profiles obtained during the wear tests on the SWNT and MWNT arrays (Bhushan *et al* 2008a).

with its tip end about ∼100 nm below the tube support layer (Bhushan *et al* 2008b). A band of amplitude attenuation formed as the tip slides on the SWNT bridge in figure 11(a). We mark three points A, B and C on the amplitude and deflection profiles across one typical scan line and illustrate possible contact geometries of the MWNT tip on the SWNT bridge for the three points in the schematic. At point A, the MWNT tip came into contact with the SWNT bridge and formed a movable junction. The vibrational energy of the AFM cantilever was dissipated partially through the friction force between the nanotubes, reducing the cantilever amplitude accordingly. Upon further scanning, the SWNT was gradually pulled while the MWNT was bent. At point B, the movable junction slipped to the end of the MWNT and the MWNT tip used its end to contact the shell of the SWNT bridge. From point B, the MWNT-end–SWNT-shell contact geometry persisted until the final detachment of nanotubes at point C, where the spring-restoring force of the nanotubes exceeded the adhesive force between nanotubes. The cantilever deflection here gives a measure of the adhesive force.

To restate, at point A, nanotubes came into contact and formed a movable junction. By analyzing the balance of the input of power and the power dissipated by the motion of the cantilever beam and by the tip–sample interaction for the vibrating cantilever, the kinetic friction between nanotubes is related to the attenuation of the cantilever amplitude as $F_{\mathrm{F}} = \pi k_z(A_0 \sin\varphi - A)/4Q$, where k_z, A_0, A and φ, Q represent the cantilever spring constant, its free amplitude, amplitude and phase during the interaction of nanotubes, and quality factor in air (Bhushan *et al* 2008b). Using the measured amplitude data during the initial contact of the nanotube, it was estimated as $F_{\mathrm{F}} = 4 \pm 1$ pN. At point B, the junction slipped to the end of the MWNT tip with the deformation of the tip. At point C, the adhesive force between nanotubes forced the nanotubes to deform more until they detached from each other. Adhesive force was calculated by multiplying the cantilever deflection at the point of detachment with the cantilever spring constant. It was estimated as $F_{\mathrm{A}} = 0.7 \pm 0.3$ nN. The coefficient of kinetic friction is calculated as $F_{\mathrm{F}}/F_{\mathrm{A}} = 0.006 \pm 0.003$. This value is comparable to values reported on graphite on a

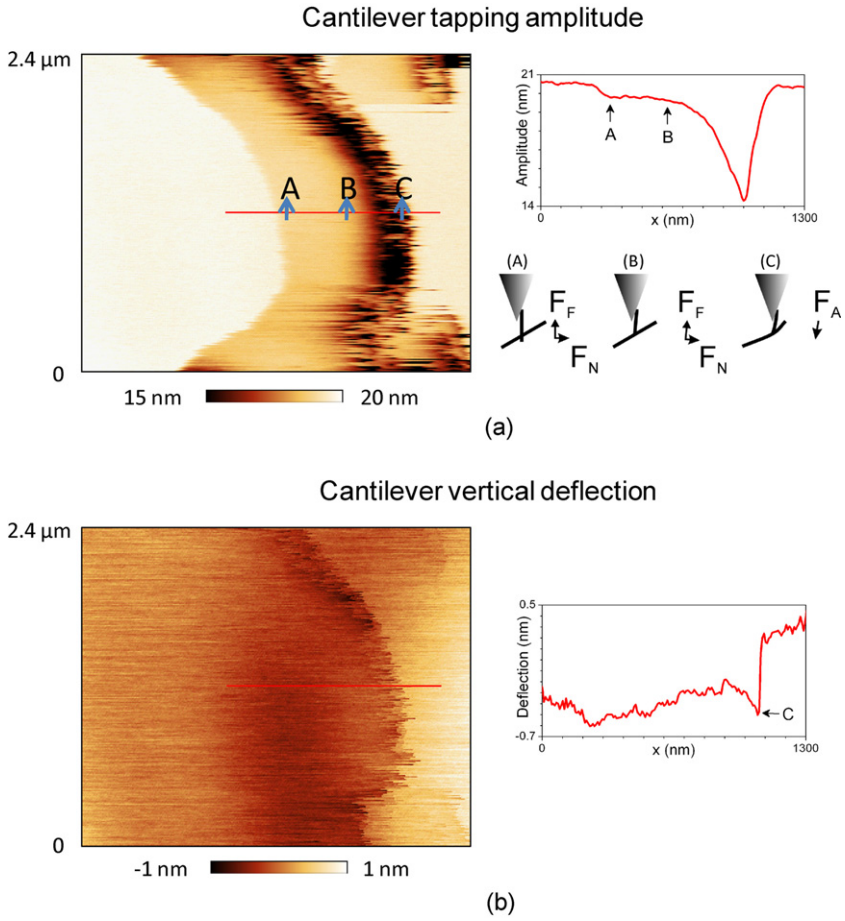

Figure 11. Images of (a) cantilever tapping amplitude and (b) cantilever vertical deflection for an MWNT tip in the tapping mode scanning in the lateral direction against an SWNT bridge. Profiles are presented next to each image for the marked scan lines which go through the suspended SWNT. The contact geometry and forces between nanotubes corresponding to the three points marked on the profiles (A, B and C) are illustrated on the right. F_F and F_N correspond to friction force and normal load, respectively. The tip end is about 100 nm lower than the tube support layer (based on Bhushan *et al* 2008b). At point A, nanotubes came into contact and formed a movable junction. At point B, the junction slipped to the end of the MWNT tip with the deformation of the tip. At point C, the adhesive force between nanotubes forces the nanotubes to deform more until they detached from each other.

nanoscale (Ruan and Bhushan 1994). With measured geometry of the nanotubes using SEM, the contact area and then the shear strength between nanotubes was estimated to be 4 ± 1 MPa using the Johnson–Kendall–Roberts model (Johnson *et al* 1971). It agrees with the value of 2 MPa reported for the sliding of MWNTs on graphite in ambient (Falvo *et al* 1999). It is also nearly two orders of magnitude larger than the interlayer shear strength of 0.05 MPa reported for MWNTs in vacuum (Kis *et al* 2006). The difference between the inter-tube and the interlayer frictions was attributed by Bhushan *et al* (2008b) to the presence of water at the nanotube–nanotube interface in ambient.

4.2. Vertical scanning

In this mode, a pristine MWNT tip freshly grown was ramped in a vertical direction against an SWNT bridge in force calibration mode to capture force versus distance curves, instead of scanning across it in a lateral direction. The latter is inappropriate for the stiff MWNT tip as it might damage the SWNT bridge during scanning (Bhushan and Ling 2008). During the scanning of an MWNT tip in the vertical direction against an SWNT bridge, in the ideal case, the MWNT tip is straight and non-deformable, and only the friction would cause the vertical deflection of the AFM cantilever to change. The vertical deflection reverses its sign when the MWNT tip switches its ramping direction from extending to retracting (and vice versa) and thus forms a friction loop, from which the friction between nanotubes is derived. In addition, during the scanning, the AFM cantilever is driven constantly by an embedded piezodriver at its resonance frequency. This enables one to acquire two additional signals, the oscillation amplitude and the phase lag of the AFM cantilever with respect to the driving force. By modeling the SWNT bridge as an elastic spring with its ends pinned at each edge of the trench, combining these signals we can estimate the contact geometry between nanotubes, specifically the displacement of the SWNT bridge, its distance and angle, from which the adhesive and friction forces, and thus the coefficient of friction between nanotubes, can be derived using the measurable vertical force.

The MWNT was ramped in the vertical direction at a ramping rate of 1–2 Hz and ramp size of several hundred

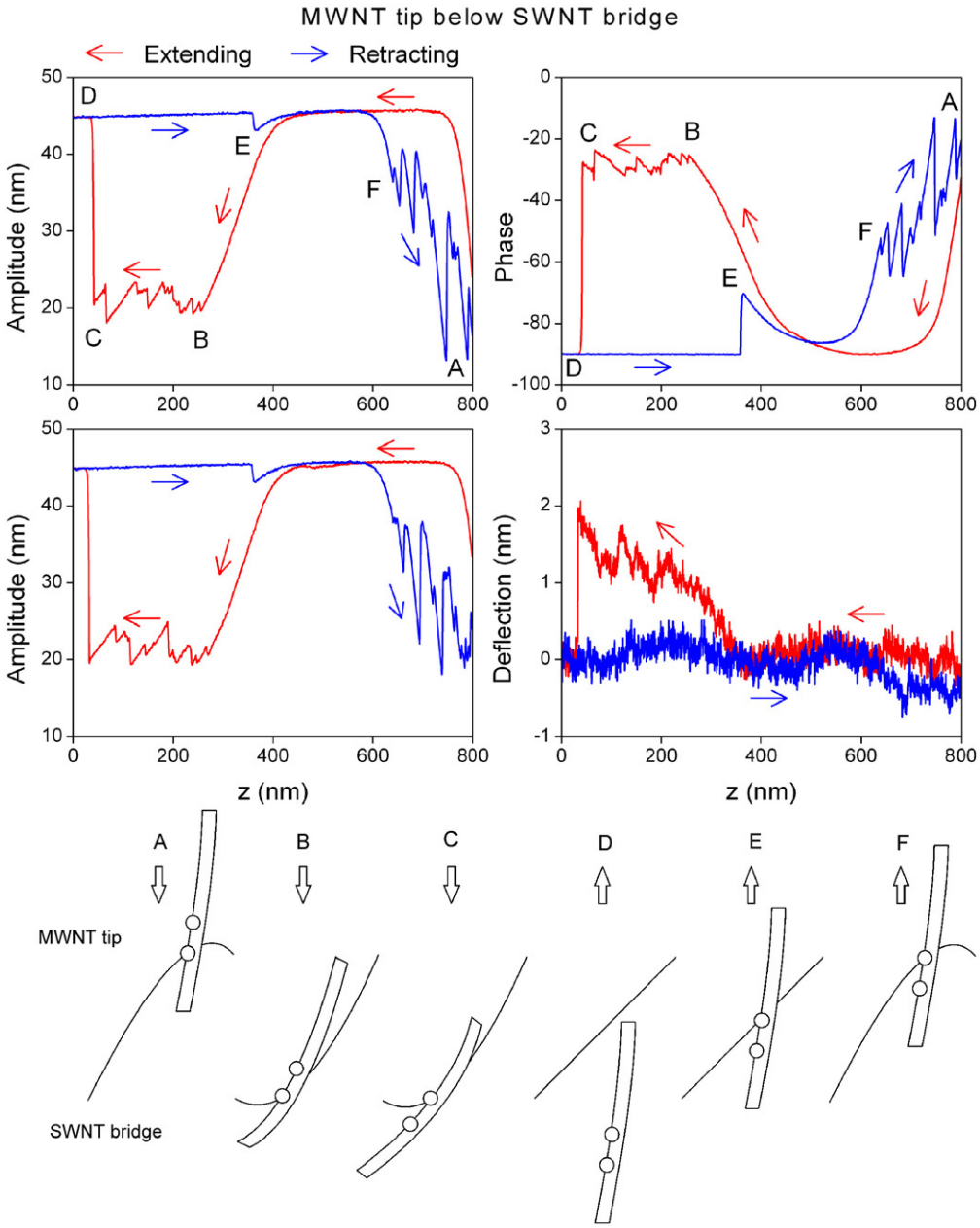

Figure 12. Typical force versus distance curves of the MWNT tip scanning in the vertical direction against an SWNT bridge from below. Oscillating amplitude, phase lag and average deflection of the cantilever as a function of ramping distance are presented. Feature points are labeled in the top plots and corresponding contact geometries of nanotubes are illustrated in the bottom schematics. The arrows in the schematics indicate the ramping direction at those points (Bhushan and Ling 2008). At points A–B: the MWNT tip stuck to the SWNT bridge; B–C: the MWNT tip slipped along the SWNT bridge; C: the MWNT tip detached the SWNT bridge; the data here are used for calculation of the adhesive force; D: the MWNT tip starts to retract; E: the MWNT tip reestablishes contact with the SWNT bridge; E–F: the MWNT tip stuck to the SWNT bridge; F–A: the MWNT tip slipped along the SWNT bridge; the data here are used for calculation of the static friction force between nanotubes.

nm. The force versus distance curves, in which the oscillation amplitude, phase lag and average deflection of the AFM cantilever are plotted against its ramping distance, are shown in figure 12 (Bhushan and Ling 2008). They were captured on two consecutive scans due to insufficient data channels available. The MWNT tip was placed below the SWNT bridge and ramped at a height range of about −500 to 300 nm with respect to the trench top. Several feature points are marked in the curve, and for each point the possible contact geometry between nanotubes is illustrated in the bottom schematics. During continuous ramping cycles, at the beginning of the extension of point A, the SWNT bridge was initially pulled up by the MWNT tip, as the oscillation amplitude of the AFM cantilever was significantly lower than its free amplitude, and its deflection was negative (downward). The contact point between nanotubes at point A is denoted by the lower circle drawn onto the MWNT tip in the schematics. With progressive extension of the MWNT tip toward the trench bottom, the

restoring force from the SWNT bridge was gradually reduced and then increased when the contact point moved below the trench top. The decrease and increase of the force between nanotubes led to the formation of an arc in the amplitude–distance curve between points A and B. After point B, the restoring force exceeded the static friction between nanotubes, and the SWNT bridge began to slip up along the MWNT tip under the effect of the restoring force.

A stick–slip motion of the SWNT bridge was expected from the observed saw-tooth pattern in the amplitude–distance curve between points B and C in figure 12. At point C, the MWNT tip was extended to a threshold such that the adhesive force between nanotubes could no longer hold them together and the two nanotubes detached from each other. The contact point between nanotubes at point of detachment C is denoted by a circle higher than the circle at which the nanotube initially contacted due to the slips between nanotubes. After detachment, the amplitude was immediately restored to the free amplitude and kept for the rest of the extension from point C to point D. At point D, the MWNT tip reversed its ramping direction and moved away from the trench bottom. Contact between the nanotubes appears to be reestablished at point E, as immediate changes to both amplitude and phase are identified. The distance between point C and point E, or the distance between the detachment and attachment of the nanotubes, clearly indicates to what extent the SWNT bridge was displaced. Although the same circle was used to denote the contact point in the schematic, it does not necessarily mean that the contact point at point E is exactly the same as that at point C. The SWNT bridge was pulled with continuous retraction, and at point F, where the contact point should be higher than the trench top, the static friction between nanotubes was overcome and the SWNT bridge began to slip down along the MWNT tip. Again, a stick–slip motion dominated the sliding between the two nanotubes between points F and A. At the end of the retraction, the contact point slipped to a point denoted by the lower circle in the schematic, where the next ramping cycle started. From the above description of a ramping cycle, we can see that the response of the cantilever at point C is a measure of the adhesive force between the shells of the nanotubes. Also, the data between points E and F can be used to evaluate the friction force, where the vertical deflection should primarily reflect the contribution from the friction force as the MWNT tip and SWNT bridge were both straightened up (Bhushan and Ling 2008).

Figure 13 shows a plot of the vertical force (normal spring constant × vertical deflection) versus the normalized amplitude obtained using 17 force versus distance curves (Bhushan and Ling 2008). The force versus distance data in the range of high and low z values in figure 12 are split into two branches in figure 13, with the low z range data corresponding to the upper branch and vice versa The static friction force estimated from the lower branch (including the data between points E and F) varied between 0 and 1.3 nN. The large noise in the deflection data, thermal noise of the order of 0.1 nN (Bhushan *et al* 2008b), combined with strong laser interference, prevents an accurate estimation of the lower limit of the static friction force, given that at point F the

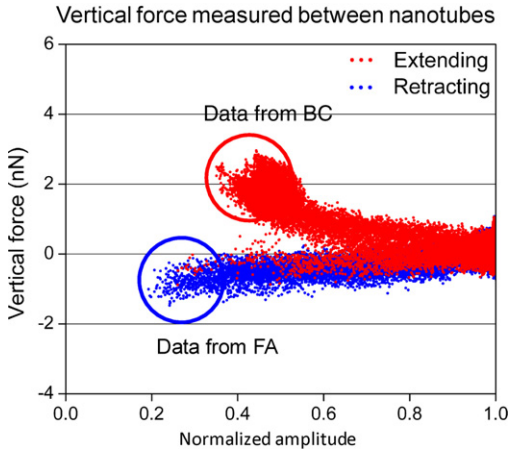

Figure 13. The interaction between nanotubes is partially detected as a vertical deflection of the AFM cantilever, from which the vertical force is calculated and plotted against normalized amplitude using 17 force versus distance curves with the MWNT tip below the SWNT bridge (based on Bhushan and Ling 2008).

amplitude is relatively large when the SWNT bridge began to slip along the MWNT tip (figure 12). The detachment of the nanotubes near the end of the extension in figure 12 allows estimation of the adhesive force between nanotubes. The vertical forces are close to 3.0 nN for the highest point, i.e. the data at point C, in figure 13. From calculations using an elastic-string modeling of the SWNT bridge, at point C the SWNT bridge would be displaced by an angle α of 60° with respect to the z axis while the MWNT tip is nearly orthogonal to the SWNT bridge (Bhushan and Ling 2008). Taking into account this information, the adhesive force between the shells of the nanotubes would be the vertical force divided by $\cos\alpha$, which equals 6.0 nN. The intershell adhesion is nearly an order of magnitude larger than the adhesion (0.7 nN) between the MWNT tip end and the SWNT shell obtained during lateral scanning, possibly due to the small radius of curvature at the MWNT tip end. Based on the upper limit of measured static friction force of 1.3 nN, the coefficient of static friction is estimated to be of the order of 0.2, nearly two orders of magnitude larger than the coefficient of kinetic friction of 0.006 obtained during lateral scanning. Lack of atomic scale periodicity in the stick–slip motion suggests the origin of friction to be high energy points (HEPs), possibly structural defects and/or coating of amorphous carbon on the surface of the pristine MWNT, rather than periodic atomic lattice (Bhushan and Ling 2008). The HEPs, which led to the 1 nN static friction during the sliding between nanotubes, were also found to be responsible for the increase of the interlayer sliding friction of MWNTs up to 1 nN (Kis *et al* 2006). While the HEPs in the interlayer sliding experiments could be dynamic due to e-beam radiation (Kis *et al* 2006), the HEPs on this MWNT tip appear to be intrinsic and permanent as the repeatability of force versus distance curves were reasonably good. This finding highlights the importance of the surface structure of nanotubes on their nanotribological properties.

The average kinetic friction force between nanotubes is estimated from the amplitude and phase data using the same

formula $F_F = \pi k_z(A_0 \sin\varphi - A)/4Q$ derived for the lateral scanning. The kinetic friction occurs during occurrence of slip between nanotubes. It was estimated to be about 20 pN (Bhushan and Ling 2008). This value is of the same order as the one reported for the lateral scanning in the previous section. A coefficient of kinetic friction of 0.003 is estimated, which is comparable to that obtained in lateral scanning. The coefficient of kinetic friction is two orders of magnitude smaller than the coefficient of static friction.

5. Concluding remarks

This paper reviews the nanotribological and nanomechanical characterization of carbon nanotubes which is fundamental for the exploration of new sliding applications. Investigation of adhesion, bending friction and wear of a multi-walled nanotube (MWNT) tip, SWNT (single-walled nanotube) and MWNT arrays has been carried out. A nonlinear response of the MWNT tip is observed when the tip is brought in and out of contact with various surfaces. Nonlinear response occurs due to the buckling of the nanotube and its subsequent sliding on the surface. In addition to the role of surface chemistry, it can also explain the relatively high value of coefficient of friction obtained on different surfaces, as compared to that of Si and Si_3N_4 tips. The adhesion and friction studies carried out on SWNT and MWNT arrays using Si tips show that SWNT arrays, as compared to MWNT arrays, exhibit lower values, possibly due to lower van der Waals forces as a result of lower packing density and higher flexibility. The adhesive force between MWNT tip and silicon substrate is measured to be ∼10 nN, about 8 times smaller than that between silicon tip and CNT array. The coefficient of friction shows the same trends as 0.04–0.06 versus 0.3.

The wear tests conducted with the MWNT tip and an Si tip on a gold film, at two normal loads, show less damage of the surface when the MWNT tip is used because of the MWNT acting as a compliant spring, absorbing part of the load. Wear tests conducted with an Si tip on SWNT and MWNT arrays show that the arrays do not wear. The tip wear and the friction force in the SWNT array are lower, because of lower adhesion and higher flexibility of the SWNTs, which are less opposed to the motion of the tip.

Adhesion and friction experiments between MWNT tip and SWNT bridge have been carried out. The coefficient of kinetic friction is 0.006. It agrees with the values measured on graphite as expected for shearing an incommensurate contact between graphite sheets. The coefficient of static friction is 0.2, about two orders of magnitude larger than the kinetic friction values. The static friction arises from structural defects and/or coating of amorphous carbon on the surface of the MWNT.

References

Baughman R H, Cui C X, Zakhidov A A, Iqbal Z, Barisci J N, Spinks G M, Wallace G G, Mazzoldi A, De Rossi D, Rinzler A G, Jaschinski O, Roth S and Kertesz M 1999 Carbon nanotube actuators *Science* **284** 1340–4

Baughman R H, Zakhidov A A and de Heer W A 2002 Carbon nanotubes—the route toward applications *Science* **297** 787–92

Belytschko T, Xiao S P, Schatz G C and Ruoff R S 2002 Atomistic simulation of nanotube fracture *Phys. Rev.* B **65** 235430

Bhushan B 2002 *Introduction to Tribology* (New York: Wiley)

Bhushan B 2003 Adhesion and stiction: mechanisms, measurement techniques, and methods for reduction *J. Vac. Sci. Technol.* B **21** 2262–96

Bhushan B 2008 *Nanotribology and Nanomechanics—An Introduction* 2nd edn (Berlin: Springer)

Bhushan B, Galasso B, Bignardi C, Nguyen C V, Dai L and Qu L 2008a Adhesion, friction and wear on nanoscale of MWNT Tips and SWNT and MWNT arrays *Nanotechnology* **19** 125702

Bhushan B and Ling X 2008 Adhesion and friction between individual carbon nanotubes measured using force-versus-distance curves in atomic force microscopy *Phys. Rev.* B **78** 045429

Bhushan B, Ling X, Jungen A and Hierold C 2008b Adhesion and friction of multiwalled carbon nanotube sliding against single-walled carbon nanotube *Phys. Rev.* B **77** 165428

Cao A, Dickrell P L, Sawyer W G, Ghasemi-Nejhad M N and Ajayan P M 2005 Super-compressible foamlike carbon nanotube films *Science* **310** 1307–10

Chen R J, Choi H C, Bangsaruntip S, Yenilmez E, Tang X, Wang Q, Chang Y L and Dai H 2004 An investigation of the mechanisms of electrode sensing of protein adsorption on carbon nanotube devices *J. Am. Chem. Soc.* **126** 1563–8

Chen Y, Shaw D T and Guo L 2000 Field emission of different oriented carbon nanotubes *Appl. Phys. Lett.* **76** 2469–71

Collins P C, Arnold M S and Avouris P 2001 Engineering carbon nanotubes and nanotube circuits using electrical breakdown *Science* **292** 706–9

Dai H J, Hafner J H, Rinzler A G, Colbert D T and Smalley R E 1996 Nanotubes as nanoprobes in scanning probe microscopy *Nature* **384** 147–50

Dalton A B, Collins S, Munoz E, Razal J M, Ebron V H, Ferraris J P, Coleman J N, Kim B G and Baughman R H 2003 Super-tough carbon-nanotube fibres—these extraordinary composite fibres can be woven into electronic textiles *Nature* **423** 703

Daraio C, Neterenko V F, Aubuchon J F and Jin S 2004a Dynamic nanofragmentation of carbon nanotubes *Nano Lett.* **4** 1915–8

Daraio C, Neterenko V F and Jin S 2004b Highly nonlinear contact interaction and dynamic energy dissipation by forest of carbon nanotubes *Appl. Phys. Lett.* **85** 5724–6

Decossas S, Cappello G, Poignant G, Patrone L, Bonnot A M, Comin F and Chevrier J 2001 Interaction forces between carbon nanotubes and an AFM tip *Europhys. Lett.* **53** 742–8

Dresselhaus M S, Dresselhaus G and Avouris P 2000 *Carbon Nanotubes: Synthesis, Structure, Properties, and Applications* (New York: Springer)

Falvo M R, Clary G J, Taylor R M, Chi V, Brooks F P, Washburn S and Superfine R 1997 Bending and buckling of carbon nanotubes under large strain *Nature* **389** 582–4

Falvo M R, Taylor R M, Helser A, Chi V, Brooks F P, Washburn S and Superfine R 1999 Nanometre-scale rolling and sliding of carbon nanotubes *Nature* **397** 236–8

Fan S, Chapline M G, Franklin N R, Tombler T W, Cassel A M and Dai H 1999 Self-oriented regular arrays of carbon nanotubes and their field emission properties *Science* **283** 512–4

Huang S D, Dai L and Mau A W H 1999 Patterned growth and contact transfer of well-aligned carbon nanotube films *J. Phys. Chem.* B **103** 4223–7

Iijima S 1991 Helical microtubules of graphitic carbon *Nature* **354** 56–8

Iijima S, Brabec C, Maiti A and Bernholc J 1995 Structural flexibility of carbon nanotubes *J. Chem. Phys.* **104** 2089–92

Jiang K L, Li Q Q and Fan S S 2002 Nanotechnology: spinning continuous carbon nanotube yarns—carbon nanotubes weave their way into a range of imaginative macroscopic applications *Nature* **419** 801

Johnson K L, Kendall K and Roberts A D 1971 Surface energy and contact of elastic solids *Proc. R. Soc.* A **324** 301–13
Jungen A, Hofmann S, Meyer J C, Stampfer C, Roth S, Robertson J and Hierold C 2007 Synthesis of individual single-walled carbon nanotube bridges controlled by support micromachining *J. Micromech. Microeng.* **17** 603–8
Jungen A, Stampfer C, Hoetzel J, Bright V M and Hierold C 2006 Process integration of carbon nanotubes into microelectromechanical systems *Sensors Actuators* A **130** 588–94
Kim P and Lieber C M 1999 Nanotube nanotweezers *Science* **286** 2148–50
Kis A, Jensen K, Aloni S, Mickelson W and Zettl A 2006 Interlayer forces and ultralow sliding friction in multiwalled carbon nanotubes *Phys. Rev. Lett.* **97** 025501–4
Larsen T, Moloni A, Flack F, Eriksson M A, Lagally M G and Black C T 2002 Comparison of wear characteristics of etched-silicon and carbon nanotube atomic-force microscopy probes *Appl. Phys. Lett.* **80** 1996–8
Lau K K S, Bico J, Teo K B K, Chhowalla M, Amaratunga G A J, Milne W I, McKinley G H and Gleason K K 2003 Superhydrophobic carbon nanotube forest *Nano Lett.* **3** 1701–5
Nakajima M, Arai F, Dong L and Fukua T 2003 Measurements of the bi-linear elasticity of identical carbon nanotubes *Nanotechnology* **1** 156–9
Nakayama Y and Akita S 2001 Field-emission device with carbon nanotubes for a flat panel display *Synth. Met.* **117** 207–10
Nguyen C V, Ye Q and Meyyappan M 2005 Carbon nanotube tips for scanning probe microscopy: fabrication and high aspect ratio nanometrology *Meas. Sci. Technol.* **16** 2138–46
Pambaguian L, Edtmainer C, Janhsen T, Ferrato M, Chereau P, Forero S, Frey T, Girmscheid A, Helbig J, Hepp F, Peigney A, Laurent C and Wulz H G 2007 Non-organic matrix materials reinforced with carbon nanotubes for space applications *Proc. Viennano '07* ed W Bartz *et al* pp 31–40
Qu L and Dai L 2007 Polymer-masking for controlled functionalization of carbon nanotubes *Chem. Commun.* **2007** 3859–61
Robertson D H, Brenner D W and Mintmire J W 1992 Energetics of nanoscale graphitic tubules *Phys. Rev.* B **45** 12592–5
Roman C, Ciontu F and Courtois B 2005 Nanoscopic modeling of a carbon nanotube force-measuring biosensor *Mol. Simul.* **31** 123–33
Ru C Q 2000 Effective bending stiffness of carbon nanotubes *Phys. Rev.* B **62** 9973–6
Ruan J A and Bhushan B 1994 Atomic-scale and micro-scale friction studies of graphite and diamond using friction force microscopy *J. Appl. Phys.* **76** 5022–35
Rueckes T, Kim K, Joselevich E, Tseng G Y, Cheung C L and Lieber C M 2000 Carbon nanotube-based nonvolatile random access memory for molecular computing *Science* **289** 94–7
Salvetat J P, Briggs G A D, Bonard J M, Bacsa R R, Kulik A J, Stockli T, Burnham N A and Forro L 1999 Elastic and shear moduli of single-walled carbon nanotube ropes *Phys. Rev. Lett.* **82** 944–7
Shaikh S, Lafdi K and Silverman E 2007 The effect of a CNT interface on the thermal resistance of contacting surfaces *Carbon* **45** 696–703
Tans S J, Verschueren A R M and Dekker C 1998 Room-temperature transistor based on a single carbon nanotube *Nature* **393** 49–52
Tao Z and Bhushan B 2006a Wetting properties of AFM probes by means of contact angle measurements *J. Phys. D: Appl. Phys.* **39** 3858–62
Tao Z and Bhushan B 2006b Surface modification of AFM Si_3N_4 probes for adhesion/friction reduction and imaging improvement *ASME J. Tribol.* **128** 865–75
Thostenson E T, Ren Z F and Chou T W 2001 Advances in the science and technology of carbon nanotubes and their composites: a review *Compos. Sci. Technol.* **61** 1899–912
Tombler T W, Zhou C, Alexseyev L, Kong J, Dai H, Liu L, Jayanthi C S, Tang M and Wu S-Y 2000 Reversible electromechanical characteristics of carbon nanotubes under local-probe manipulation *Nature* **405** 769–72
Treacy M M J, Ebbesen T W and Gibson J M 1996 Exceptionally high Young's modulus observed for individual carbon nanotubes *Nature* **381** 678–80
Vigolo B, Penicaud A, Coulon C, Sauder C, Pailler R, Journet C, Bernier P and Poulin P 2000 Macroscopic fibers and ribbons of oriented carbon nanotubes *Science* **290** 1331–4
Wildoer J W G, Venema L C, Rinzler A G, Smalley R E and Dekker C 1998 Electronic structure of atomically resolved carbon nanotubes *Nature* **391** 59–62
Wong E W, Sheenan P E and Lieber C M 1997 Nanobeam mechanics: elasticity, strength and toughness of nanorods and nanotubes *Science* **277** 1971–5
Wong S S, Joselevich E, Woolley A T, Cheung C L and Lieber C M 1998 Covalently functionalized nanotubes as nanometre-sized probes in chemistry and biology *Nature* **394** 52–5
Yakobson B I, Brabec C J and Bernholc J 1996 Nanomechanics of carbon tubes: instabilities beyond linear response *Phys. Rev. Lett.* **76** 2511–4
Young W C and Budynas R G 2002 *Roark's Formulas for Stress and Strain* 7th edn (New York: McGraw-Hill)
Yu M-F, Lourie O, Dyer M J, Moloni K, Kelly T F and Ruoff R S 2000 Strength and breaking mechanism of multiwalled carbon nanotubes under tensile load *Science* **287** 637–40
Yurdumakan B, Raravikar N R, Ajayan P M and Dhinojwala A 2005 Synthetic Gecko Foot-Hairs from multiwalled carbon nanotubes *Chem. Commun.* **2005** 3799–801
Zhang M, Fang S, Zakhidov A A, Lee S B, Aliev A E, Williams C D, Atkinson K R and Baughman R H 2005 Strong, transparent, multifunctional, carbon nanotube sheets *Science* **309** 1215–9